Progress In Electromagnetics Research C, Vol. 81, 161–169, 2018

Estimation of Motion Parameters with Dual-frequency InSAR Imaging Technique

Kai-Shiun Yang, Po-Chih Chen, and Jean-Fu Kiang*

Abstract—A dual-frequency InSAR imaging technique is proposed to estimate the position and motion parameters of a moving target, including velocity and cross-track acceleration. Conventional methods of estimating the velocity and acceleration of a moving target, from the phase information of bistatic SAR signal, are usually compromised by phase ambiguity. By applying the dual-frequency technique, phase ambiguity is effectively removed to ascertain accurate estimation of motion parameters. In addition, an alternative method is proposed to estimate different velocity components, by taking higher-order terms and solving coupled linear equations of the velocity components. The simulation results verify that the errors of velocity and acceleration are less than 1 m/s and 0.25 m/s^2, respectively.

1. INTRODUCTION

Various approaches, synthetic aperture radar (SAR) imaging techniques, have been proposed to estimate the velocity and acceleration of a ground moving target. The range cell migration (RCM) in the received signal of a moving target spreads to more range cells than that of a static target. The motion parameters can be estimated more accurately if the range cell migration compensation (RCMC) can be conducted more effectively.

Keystone transform has been used to compensate RCM [1], range walk migration [2] and range curvature migration [3]. However, when a target moves at high cross-track speed, the keystone transform may fail to compensate the RCM completely due to Doppler ambiguity of the target motion [4]. Thus, an azimuth-dechirping algorithm was applied before taking the keystone transform, and RCMC was carried out successfully to process multiple targets at high range velocity.

The keystone transform can correct severe range curvature which may occur at short ranges [5]. In [6, 7], a range curvature filter was applied to compensate the RCM, under the assumption that the azimuth velocity of the target is small compared to the platform velocity and the target does not accelerate. Usually, an RCMC filter works fine when Doppler ambiguity is present, but may fail if the along-track velocity is not negligible. When the target appears at a short slant range, the filter may fail more easily even if the target moves at a slow along-track speed. In [8, 9], a Doppler ambiguity-free approach, based on Radon transform, was applied to estimate the range velocity by processing the range walk in both the fast and the slow time domains. In [10], a velocity correlation function (VCF) was proposed to estimate the range velocity and azimuth velocity, and the latter is estimated more accurately than the former.

The phase of SAR signals can be represented as a polynomial phase signal (PPS). A general ambiguity function (GAF) [11] or high-order ambiguity function (HAF) [12] can then be applied to estimate the coefficients of the PPS. In [6], a GAF was applied to find the range acceleration and azimuth velocity of a moving target. In [13], a Wigner-ville distribution (WVD) was applied to find the azimuth chirp rate, from which the along-track velocity was estimated. In [14], a fractional Fourier

Received 6 November 2017, Accepted 12 February 2018, Scheduled 19 February 2018
* Corresponding author: Jean-Fu Kiang (jfkiang@ntu.edu.tw).
The authors are with the Graduate Institute of Communication Engineering, National Taiwan University, Taipei, Taiwan, R.O.C.

transform (FrFT) was applied to estimate the azimuth chirp rate by concentrating the energy of a chirp signal.

Doppler ambiguity occurs frequently in mm-wave SAR, in which the Doppler frequency of a moving target is often larger than the pulse repetition frequency (PRF). In [15], a ground moving target indication (GMTI) based on a dual-frequency SAR was proposed. By choosing a co-prime wavelength, range velocity less than 110 m/s can be uniquely determined. In [16], an unambiguous slant-range velocity estimation algorithm and two other methods for azimuth compression were proposed. The resolution of carrier-phase ambiguity is also an important issue in the global navigation satellite system (GNSS). In [17], a three-carrier ambiguity resolution (TCAR) was proposed by utilizing a linear combination of signals at different frequencies.

In this work, a dual-frequency SAR imaging technique is proposed to estimate the position and motion parameters of a moving target, including along-track and cross-track velocity components as well as cross-track acceleration. The proposed method can be applied to missions with high squint angles. This paper is organized as follows. The proposed InSAR model is presented in Section 2. The estimation approach of position and motion parameters are presented in Section 3. The dual-frequency technique for resolving phase ambiguity is presented in Section 4. An alternative method to estimate velocity components is derived in Section 5. The simulation results are discussed in Section 6. Finally, some conclusions are drawn in Section 7.

2. PROPOSED INSAR MODEL

Figure 1 shows the schematic of dual-receiver along-track interferometric SAR (InSAR), and Fig. 2 shows the flowchart to estimate the motion parameters [18]. In conventional methods, the along-track velocity is estimated first, and the cross-track velocity is then estimated by using the along-track velocity just acquired. In this work, by including more higher-order terms that were neglected in the conventional methods, the along-track and the cross-track velocity components can be estimated simultaneously by solving coupled linear equations of these velocity components.

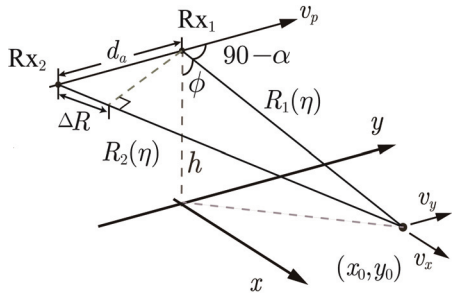

Figure 1. Schematic of dual-receiver InSAR [18].

The received signals after demodulation can be represented as

$$\begin{aligned} s_{1\mathrm{rb}}(\tau,\eta) &= A_0 w_r\left(\tau - 2R_1(\eta)/c\right) e^{j2\pi f_0[\tau-2R_1(\eta)/c]+j\pi K_r[\tau-2R_1(\eta)/c]^2} + n_r(\tau,\eta) \\ s_{2\mathrm{rb}}(\tau,\eta) &= A_0 w_r\left(\tau - [R_1(\eta)+R_2(\eta)]/c\right) e^{j2\pi f_0\{\tau-[R_1(\eta)+R_2(\eta)]/c\}+j\pi K_r\{\tau-[R_1(\eta)+R_2(\eta)]/c\}^2} + n_r(\tau,\eta) \end{aligned}$$

where $R_1(\eta)$ and $R_2(\eta)$ are the slant ranges from Rx_1 and Rx_2, respectively, to the target, and $n_r(\tau,\eta)$ is white Gaussian noise with zero mean and variance σ^2. The signal-to-noise ratio is defined as $10\log_{10}(A_0^2/\sigma^2)$, and A_0 is set to unity without loss of generality.

The received signals after range compression can be represented as

$$\begin{aligned} s_{1\mathrm{rc}}(\tau,\eta) &= e^{-j4\pi f_0 R_1(\eta)/c}\mathrm{sinc}(B_r(\tau - 2R_1(\eta)/c)) \\ s_{2\mathrm{rc}}(\tau,\eta) &= e^{-j2\pi f_0[R_1(\eta)+R_2(\eta)]/c}\mathrm{sinc}\left(B_r\left[\tau - [R_1(\eta)+R_2(\eta)]/c\right]\right) \\ &\simeq e^{-j2\pi f_0[2R_1(\eta)+\Delta R(\eta)]/c}\mathrm{sinc}\left(B_r\{\tau - [2R_1(\eta)+\Delta R(\eta)]/c\}\right) \end{aligned} \quad (1)$$

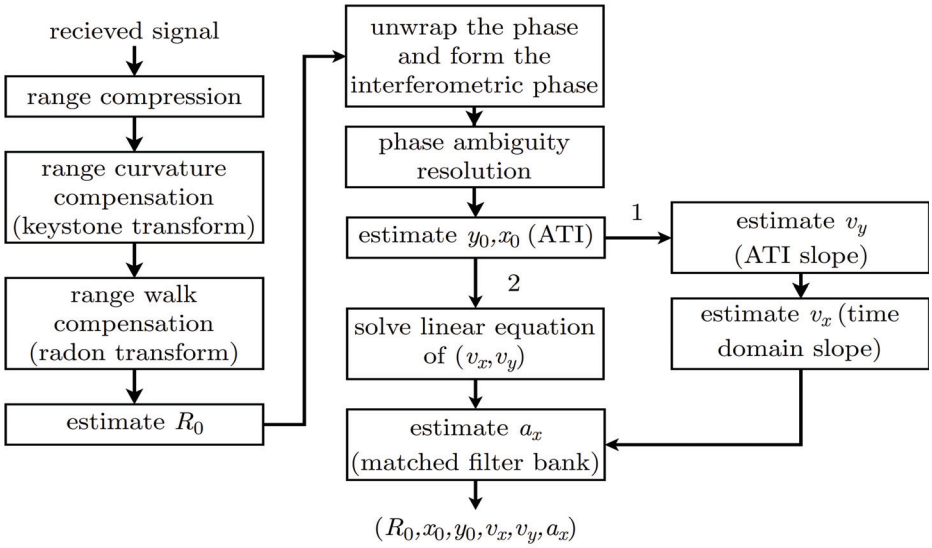

Figure 2. Flowchart to estimate motion parameters. Process 2 marks the proposed method which is different from process 1 [18].

where B_r is the bandwidth of the chirp signal and $\Delta R(\eta) = R_2(\eta) - R_1(\eta)$. The slant range $R_1(\eta)$ is expanded up to the second order of η as

$$R_1(\eta) \simeq R_0 + \frac{v_x x_0 - y_0(v_p - v_y)}{R_0}\eta + \frac{(v_p - v_y)^2 + a_x x_0}{2R_0}\eta^2$$

then $\Delta R(\eta)$ is approximated as

$$\Delta R(\eta) \simeq d_a \sin\alpha \simeq d_a\left(\frac{y_0}{R_0} - \frac{v_p - v_y}{R_0}\eta\right) \tag{2}$$

where d_a is the distance between Rx_1 and Rx_2. By taking the Fourier transform of $s_{1\mathrm{rc}}(\tau,\eta)$ and $s_{2\mathrm{rc}}(\tau,\eta)$ with respect to τ, we obtain

$$\begin{aligned}
S_{1\mathrm{rc}}(f_\tau,\eta) &= A_1 w_a(\eta) W_r(f_\tau)\exp\left\{-j4\pi\frac{f_0+f_\tau}{c}\left[R_0 + \frac{v_x x_0 - y_0(v_p-v_y)}{R_0}\eta + \frac{(v_p-v_y)^2 + a_x x_0}{2R_0}\eta^2\right]\right\}\\
S_{2\mathrm{rc}}(f_\tau,\eta) &= A_1 w_a(\eta) W_r(f_\tau)\exp\left\{-j4\pi\frac{f_0+f_\tau}{c}\left[R_0 + \frac{\Delta R(\eta)}{2} + \frac{v_x x_0 - y_0(v_p-v_y)}{R_0}\eta\right.\right.\\
&\quad \left.\left. + \frac{(v_p-v_y)^2 + a_x x_0}{2R_0}\eta^2\right]\right\}
\end{aligned}$$

where A_1 is a constant independent of either τ or η.

Next, applying the second-order keystone transform to $S_{1\mathrm{rc}}(f_\tau,\eta)$ and $S_{2\mathrm{rc}}(f_\tau,\eta)$, with $\eta^2 = \dfrac{f_0}{f_0+f_\tau}t^2$, we have

$$\begin{aligned}
S_{1k}(f_\tau,t) &\simeq A_1 w_a(t) W_r(f_\tau)\exp\left\{-j\frac{4\pi}{c}\left[(f_0+f_\tau)R_0 + \left(f_0+\frac{f_\tau}{2}\right)\frac{v_x x_0 - y_0(v_p-v_y)}{R_0}t\right.\right.\\
&\quad \left.\left. + f_0\frac{(v_y-v_p)^2 + a_x x_0}{2R_0}t^2\right]\right\}\\
S_{2k}(f_\tau,t) &\simeq A_1 w_a(t) W_r(f_\tau)\exp\left\{-j\frac{4\pi}{c}\left[(f_0+f_\tau)\left(R_0 + \frac{1}{2}\frac{d_a y_0}{R_0}\right)\right.\right.\\
&\quad \left.\left. + \left(f_0+\frac{f_\tau}{2}\right)\left[-\frac{1}{2}\frac{d_a(v_p-v_y)}{R_0} + \frac{v_x x_0 - y_0(v_p-v_y)}{R_0}\right]t + f_0\frac{(v_y-v_p)^2 + a_x x_0}{2R_0}t^2\right]\right\}
\end{aligned}$$

By taking the inverse Fourier transform of $S_{1k}(f_\tau, t)$ and $S_{2k}(f_\tau, t)$ with respect to f_τ, we obtain

$$\begin{aligned} s_{1k}(\tau,t) &= A_1 w_a(t)\mathrm{sinc}\left(B_r\left\{\tau-\frac{2}{c}\left[R_0+\frac{v_x x_0-y_0(v_p-v_y)}{2R_0}t\right]\right\}\right) \\ &\quad \exp\left\{-j\frac{4\pi f_0}{c}\left[R_0+\frac{v_x x_0-y_0(v_p-v_y)}{R_0}t+\frac{(v_y-v_p)^2+a_x x_0}{2R_0}t^2\right]\right\} \\ s_{2k}(\tau,t) &= A_1 w_a(t)\mathrm{sinc}\left(B_r\left\{\tau-\frac{2}{c}\left[R_0+\frac{v_x x_0-y_0(v_p-v_y)}{2R_0}t+\frac{d_a y_0}{2R_0}-\frac{d_a(v_p-v_y)}{4R_0}t\right]\right\}\right) \\ &\quad \exp\left\{-j\frac{4\pi f_0}{c}\left[R_0-\frac{1}{2}\frac{d_a(v_p-v_y)}{R_0}t+\frac{1}{2}\frac{d_a y_0}{R_0}+\frac{v_x x_0-y_0(v_p-v_y)}{R_0}t+\frac{(v_y-v_p)^2+a_x x_0}{2R_0}t^2\right]\right\} \end{aligned}$$

The argument in the sinc function depicts a linear equation in the τ-t plane, with a slope of

$$\ell_{\tau t}=\frac{cR_0}{v_x x_0-y_0(v_p-v_y)} \tag{3}$$

which is numerically extracted by applying a Radon transform to $s_{1k}(\tau, t)$.

To implement range walk migration compensation, a range walk filter, $H_w(f_\tau, t) = e^{j2\pi f_\tau t/\ell_{\tau t}}$, is applied to $S_{1k}(f_\tau, t)$ and $S_{2k}(f_\tau, t)$ to obtain

$$\begin{aligned} S_{1c}(f_\tau,t) &= S_{1k}(f_\tau,t)H_w(f_\tau,t) \\ &= A_1 w_a(t)W_r(f_\tau)\exp\left\{-j\frac{4\pi}{c}\left[(f_0+f_\tau)R_0+f_0\frac{v_x x_0-y_0(v_p-v_y)}{R_0}t+f_0\frac{(v_y-v_p)^2+a_x x_0}{2R_0}t^2\right]\right\} \\ S_{2c}(f_\tau,t) &= S_{2k}(f_\tau,t)H_w(f_\tau,t) = A_1 w_a(t)W_r(f_\tau)\exp\left\{-j\frac{4\pi}{c}\left[(f_0+f_\tau)\left(R_0+\frac{d_a y_0}{2R_0}\right)\right.\right. \\ &\quad \left.\left.-(f_0+f_\tau/2)\frac{1}{2}\frac{d_a(v_p-v_y)}{R_0}t+f_0\frac{v_x x_0-y_0(v_p-v_y)}{R_0}t+f_0\frac{(v_y-v_p)^2+a_x x_0}{2R_0}t^2\right]\right\} \end{aligned}$$

By taking the inverse Fourier transform of $S_{1c}(f_\tau, t)$ and $S_{2c}(f_\tau, t)$ with respect to f_τ, we obtain

$$\begin{aligned} s_{1c}(\tau,t) &= A_1 w_a(t)\,\mathrm{sinc}(B_r(\tau-2R_0/c))\exp\left\{-j\frac{4\pi f_0}{c}\phi(t)\right\} \\ s_{2c}(\tau,t) &= A_1 w_a(t)\,\mathrm{sinc}\left(B_r\left[\tau-\frac{2R_0}{c}-\frac{d_a y_0}{cR_0}+\frac{d_a(v_p-v_y)}{2cR_0}t\right]\right)\exp\left\{-j\frac{4\pi f_0}{c}\left[\phi(t)+\frac{d_a y_0}{2R_0}-\frac{d_a(v_p-v_y)}{2R_0}t\right]\right\} \\ &\simeq A_1 w_a(t)\,\mathrm{sinc}(B_r(\tau-2R_0/c))\exp\left\{-j\frac{4\pi f_0}{c}\left[\phi(t)+\frac{d_a y_0}{2R_0}-\frac{d_a(v_p-v_y)}{2R_0}t\right]\right\} \end{aligned}$$

where

$$\phi(t)=R_0+\frac{v_x x_0-y_0(v_p-v_y)}{R_0}t+\frac{(v_y-v_p)^2+a_x x_0}{2R_0}t^2$$

3. ESTIMATION OF POSITION AND MOTION PARAMETERS

The maximum amplitude of $s_{1c}(\tau, t)$ occurs at $\tau = \tau_p$, where the argument of sinc function is equal to zero, namely, $\tau_p - 2R_0/c = 0$. Thus, R_0 is estimated as $\tilde{R}_0 = c\tilde{\tau}_p/2$.

By taking Rx_1 as the reference and multiplying $s_{1c}(\tau = 2R_0/c, t)$ with $s^*_{2c}(\tau = 2R_0/c, t)$ [18], an interferometric intensity is derived as

$$I(t)=s_{1c}\left(\tau=2R_0/c,t\right)s^*_{2c}\left(\tau=2R_0/c,t\right)=w_a^2(t)e^{j\varphi(t)} \tag{4}$$

where

$$\varphi(t)=\frac{4\pi f_0}{c}\left[\frac{d_a y_0}{2R_0}-\frac{d_a(v_p-v_y)}{2R_0}t\right] \tag{5}$$

From $\varphi(0) = \dfrac{4\pi f_0}{c}\dfrac{d_a}{2R_0}y_0$, y_0 can be estimated as $\tilde{y}_0 = \dfrac{c\tilde{R}_0}{2\pi f_0 d_a}\varphi(0)$. Based on $\tilde{R}_0$ and $\tilde{y}_0$, x_0 is estimated as $\tilde{x}_0 = \sqrt{\tilde{R}_0^2 - h^2 - \tilde{y}_0^2}$.

The slope of phase angle $\varphi(t)$ in Eq. (5) versus t is $\ell = -\dfrac{4\pi f_0}{c}\dfrac{d_a(v_p - v_y)}{2R_0}$. The slope $\tilde{\ell}$ is numerically extracted and used to estimate v_y as

$$\tilde{v}_y = v_p + \tilde{\ell}\frac{c}{2\pi f_0}\frac{\tilde{R}_0}{d_a} \tag{6}$$

The signal $S_{1c}(f_\tau, t)$ can be rewritten as

$$S_{1c}(f_\tau, t) = A_1 w_a(t) W_r(f_\tau) \exp\left\{-j\frac{4\pi}{c}(f_0 + f_\tau)R_0 + j\alpha_1 t + j\alpha_2 t^2\right\} \tag{7}$$

where

$$\alpha_1 = -\frac{4\pi}{c}f_0\frac{v_x x_0 - y_0(v_p - v_y)}{R_0}, \quad \alpha_2 = -\frac{4\pi}{c}f_0\frac{(v_y - v_p)^2 + a_x x_0}{2R_0}$$

The value of a_x is estimated from the expression of α_2 as

$$\tilde{a}_x = \frac{1}{\tilde{x}_0}\left[-\tilde{\alpha}_2\frac{c\tilde{R}_0}{2\pi f_0} - (\tilde{v}_y - v_p)^2\right] \tag{8}$$

where $\tilde{\alpha}_2$ is the estimated value of α_2.

The value of v_x can be estimated from the slope in Eq. (3) as

$$\tilde{v}_x = \frac{1}{\tilde{x}_0}\left[\frac{c\tilde{R}_0}{\tilde{\ell}_{\tau t}} + \tilde{y}_0(v_p - \tilde{v}_y)\right] \tag{9}$$

It can also be estimated in an alternative way. Define a second-order compensation filter, $H_2(f_\tau, t) = e^{-j\alpha_2 t^2}$, which is applied to $S_{1c}(f_\tau, t)$ to derive

$$S'_{1c}(f_\tau, t) = S_{1c}(f_\tau, t)H_2(f_\tau, t) = A_1 w_a(t) W_r(f_\tau)\exp\left\{-j\frac{4\pi}{c}(f_0 + f_\tau)R_0 + j\alpha_1 t\right\}$$

where $\alpha_1 = -\dfrac{4\pi}{c}f_0\dfrac{v_x x_0 - y_0(v_p - v_y)}{R_0}$ is the slope of phase of $S'_{1c}(f_\tau, t)$ versus t. The slope, $\tilde{\alpha}_1$, is numerically extracted and then used to estimate v_x as

$$\tilde{v}_x = \frac{1}{\tilde{x}_0}\left[-\tilde{\alpha}_1\frac{c\tilde{R}_0}{4\pi f_0} + \tilde{y}_0(v_p - \tilde{v}_y)\right] \tag{10}$$

The value of v_x can be estimated by using Eq. (9) or (10), which are derived from the amplitude of $s_{1k}(\tau, t)$ and the phase of $S'_{1c}(f_\tau, t)$, respectively. Empirically, the phase information is more reliable than the amplitude information.

4. DUAL-FREQUENCY TECHNIQUE FOR RESOLVING PHASE AMBIGUITY

When using $\varphi(0)$ in Eq. (5) to estimate y_0, the phase ambiguity may result in an erroneous estimation as

$$\varphi(0) = \beta\tilde{y}_{0m} + 2N\pi$$

where $\beta = \dfrac{2\pi f_0 d_a}{cR_0}$, $\tilde{y}_{0m}$ is an ambiguous azimuth position, and N is an ambiguity number. The phase ambiguity will be resolved by applying a dual-frequency technique. Consider two LFM signals with carrier frequencies of f_{c1} and f_{c2}, respectively, with $f_{c1} > f_{c2}$. LFM signals at the difference frequency

$f_d = f_{c1} - f_{c2}$ and the sum frequency $f_s = f_{c1} + f_{c2}$ are also available via intermodulation. Thus, the phase at $t = 0$ in Eq. (5), at one of the four different frequencies, is

$$\varphi_\alpha(0) = \frac{2\pi f_\alpha d_a}{cR_0} y_0 = \beta_\alpha \tilde{y}_{0\alpha} + 2N_\alpha \pi \tag{11}$$

with $\alpha = c1, c2, s, d$, where $\varphi_\alpha(0)$ and N_α are the phase and ambiguity number, respectively, at frequency f_α, and $\beta_\alpha = \dfrac{2\pi f_\alpha d_a}{cR_0}$. Eq. (11) implies that y_0 satisfies

$$\frac{2\pi d_a}{R_0} y_0 = (\beta_{c1}\tilde{y}_{0c1} + 2N_{c1}\pi)\,\lambda_{c1} = (\beta_{c2}\tilde{y}_{0c2} + 2N_{c2}\pi)\,\lambda_{c2} = (\beta_s \tilde{y}_{0s} + 2N_s\pi)\,\lambda_s = (\beta_d \tilde{y}_{0d} + 2N_d\pi)\,\lambda_d \tag{12}$$

where $\lambda_\alpha = c/f_\alpha$ is the wavelength at frequency f_α.

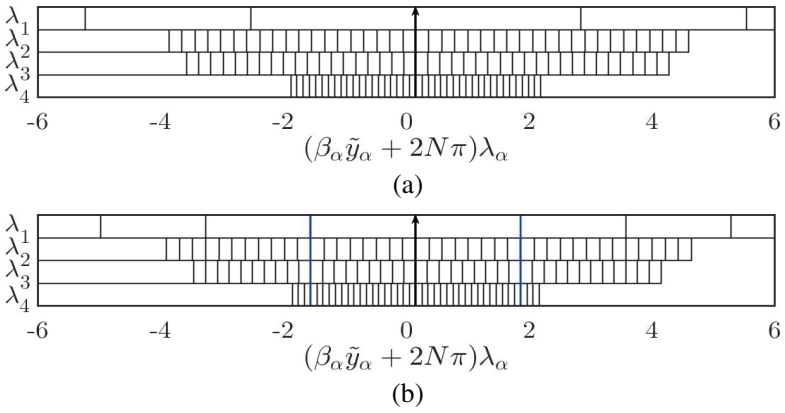

Figure 3. Possible values of $(\beta_\alpha \tilde{y}_\alpha + 2N_\alpha\pi)\lambda_\alpha$, (a) $(f_1, f_2, f_3, f_4) = (0.7, 8.9, 9.6, 18.5)$ GHz, (b) $(f_1, f_2, f_3, f_4) = (1.1, 8.8, 9.9, 18.7)$ GHz. Black arrow marks correct estimation and blue lines mark erroneous estimations.

Proper selection of carrier frequencies is critical to resolve the ambiguity. Fig. 3 demonstrates how to select proper carrier frequencies. At first, a pair of f_{c1} and f_{c2} are empirically chosen. Then, they are sorted with f_s and f_d, then relabeled as f_1, f_2, f_3 and f_4, in an ascending order. Fig. 3 shows possible values of $(\beta_\alpha \tilde{y}_\alpha + 2N_\alpha\pi)\lambda_\alpha$ at all the four frequencies. Note that $f_4 = f_s$ is relatively higher than the others, and $f_1 = f_d$ is relatively lower than the others. Thus, it is convenient to use possible values at f_1 to determine if the selection of frequencies is proper. Fig. 3(a) illustrates an obvious candidate of ambiguity number, while Fig. 3(b) shows multiple candidates, which may lead to an incorrect estimation of y_0, especially in the presence of noise.

A rule of thumb for frequency selection is to make possible values of $(\beta_\alpha \tilde{y}_\alpha + 2N_\alpha\pi)\lambda_\alpha$ aligned at only one ambiguity number. In practice, f_{c1} and f_{c2} are selected to satisfy

$$f_{c1} \bmod f_d \simeq f_d/2, \quad f_{c2} \bmod f_d \simeq f_d/2$$

5. ALTERNATIVE METHOD TO ESTIMATE VELOCITY

Equation (2) can be expanded in an alternative way as

$$\Delta R(\eta) = d_a \left\{ \frac{y_0}{R_0} - \eta \left[\frac{v_p - v_y}{R_0} + y_0 \frac{v_x x_0 - y_0(v_p - v_y)}{R_0^3} \right] \right\} \tag{13}$$

Then, the phase in the interferometric intensity, defined in Eq. (4), becomes

$$\varphi(t) = \frac{4\pi f_0}{c} \left\{ \frac{d_a y_0}{2R_0} - \left[\frac{v_p - v_y}{2R_0} + y_0 \frac{v_x x_0 - y_0(v_p - v_y)}{2R_0^3} \right] t \right\} \tag{14}$$

which implies a slope of

$$\ell = -\frac{2\pi f_0 d_a}{c}\left[\frac{v_p - v_y}{R_0} + y_0\frac{v_x x_0 - y_0(v_p - v_y)}{R_0^3}\right] \tag{15}$$

In contrast to the previous approach of estimating v_y first, then using the estimated v_y to estimate v_x, here, Eqs. (3) and (15) are reorganized as

$$\begin{aligned} v_x + \frac{y_0}{x_0}v_y &= \frac{1}{x_0}\left(\frac{cR_0}{\ell_{\tau t}} + y_0 v_p\right) \\ -\frac{x_0 y_0}{R_0^3}v_x + \left(\frac{1}{R_0} - \frac{y_0^2}{R_0^3}\right)v_y &= \frac{v_p}{R_0} - \frac{y_0^2 v_p}{R_0^3} + \frac{c}{2\pi f_0 d_a}\ell \end{aligned} \tag{16}$$

which are then solved simultaneously for v_x and v_y.

6. SIMULATIONS AND DISCUSSIONS

Table 1 lists the parameters of an X-band InSAR mission [18]. The acceleration is fixed at $a_x = 3\ \mathrm{m}/s^2$, and both the cross-track and along-track velocities are varied in the range from -20 to $20\,\mathrm{m/s}$.

Table 1. Parameters of X-band InSAR mission [18].

parameter	symbol	magnitude	unit
first carrier frequency	f_{c1}	9.6	GHz
second carrier frequency	f_{c2}	8.9	GHz
light speed	c	299,792,458	m/s
pulse length	T_p	5	μs
chirp rate	K_r	1×10^{13}	$1/\mathrm{s}^2$
bandwidth	B_r	50	MHz
fast time sampling frequency	$1/(4B_r)$	200	MHz
number of range samples	N_r	2,048	
pulse repetition frequency	PRF	4,000	Hz
number of azimuth samples	N_a	2,048	
antenna separation	d_a	1	m
center range	R_0	3,111	m
platform height	h	2,200	m
platform velocity	v_p	90	m/s
exposure time	T_a	2	s
look angle	ϕ	45	deg.
squint angle	α	7	deg.

Figure 4 shows the error of $\tilde{v}_x$ at different v_xs and v_ys. By applying Eqs. (9) and (16), larger error occurs when v_x is larger than $10\,\mathrm{m/s}$. Otherwise, the error is less than $1\,\mathrm{m/s}$. It is also observed that the estimation error by using Eq. (10) is smaller than those obtained by using Eq. (9) or (16).

Figure 5 shows the error of $\tilde{v}_y$ at different v_xs and v_ys. The error with Eq. (6) is larger than that with Eq. (16). The error of applying Eq. (6) also displays a large offset and linear trend with respect to both v_x in Fig. 5(a) and v_y in Fig. 5(b).

Figure 6 shows the error of $\tilde{a}_x$ at different v_xs and v_ys. It is observed that the estimated a_x is always smaller than $0.25\,\mathrm{m/s}^2$ with both methods.

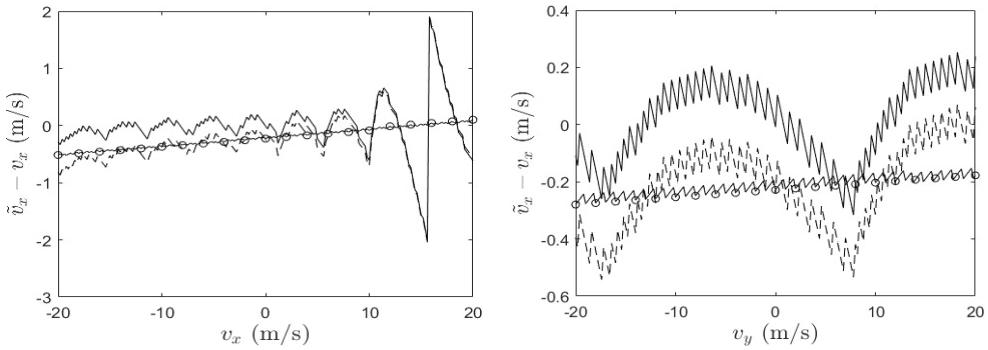

Figure 4. Error of $\tilde{v}_x$, (a) $v_y = 0\,\mathrm{m/s}$, (b) $v_x = 0\,\mathrm{m/s}$, ——: with (16), − − −: with (9), − ∘ −: with (10).

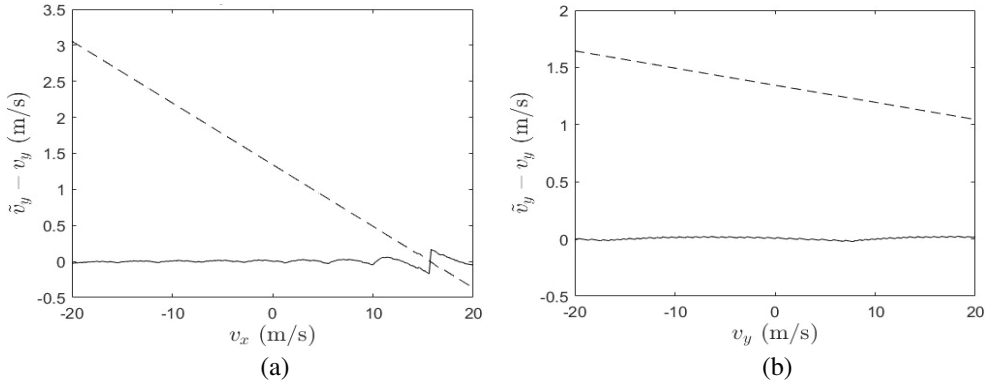

Figure 5. Error of $\tilde{v}_y$, (a) $v_y = 0\,\mathrm{m/s}$, (b) $v_x = 0\,\mathrm{m/s}$, ——: with (16), − − −: with (6).

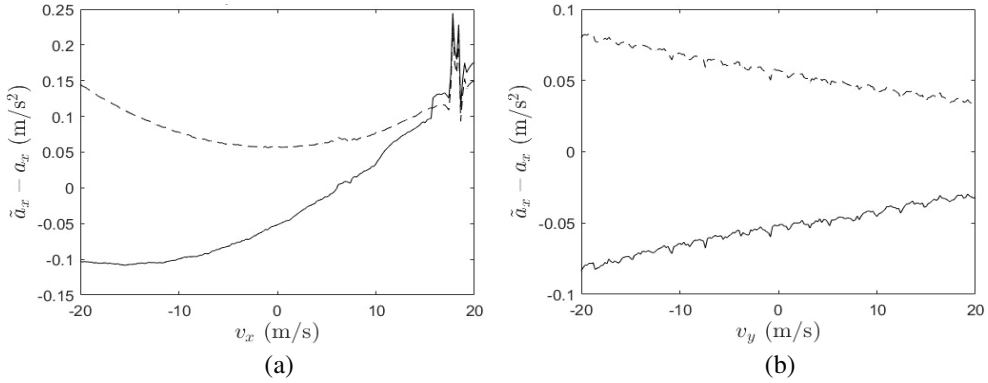

Figure 6. Error of $\tilde{a}_x$, (a) $v_y = 0\,\mathrm{m/s}$, (b) $v_x = 0\,\mathrm{m/s}$, ——: substituting the values obtained from (6) into (8), − − −: with (8).

7. CONCLUSION

A dual-frequency InSAR imaging technique is proposed to estimate the position and motion parameters of a moving target, including along-track and cross-track velocity components as well as cross-track acceleration. By applying the dual-frequency technique, phase ambiguity is effectively removed to ascertain accurate estimation of the motion parameters. In addition, an alternative method is proposed to estimate both velocity components, by including more higher-order terms and simultaneously solving coupled linear equations of both velocity components. The simulation results demonstrate that the errors of velocity and acceleration are less than $1\,\mathrm{m/s}$ and $0.25\,\mathrm{m/s^2}$, respectively.

REFERENCES

1. Perry, R. P., R. C. Dipietro, and R. L. Fante, "SAR imaging of moving targets," *IEEE Trans. Aero. Electron. Syst.*, Vol. 35, 188–200, 1999.
2. Jungang, Y., H. Xiaotao, J. Tian, J. Thompson, and Z. Zhimin, "New approach for SAR imaging of ground moving targets based on a keystone transform," *IEEE Geosci. Remote Sensing Lett.*, Vol. 8, 829–833, 2011.
3. Huang, P., G. Liao, Z. Yang, X. G. Xia, J. Ma, and J. Zheng, "Ground maneuvering target imaging and high-order motion parameter estimation based on second-order keystone and generalized Hough-HAF transform," *IEEE Trans. Geosci. Remote Sensing*, Vol. 55, 320–335, 2017.
4. Yang, J. and Y. Zhang, "An airborne SAR moving target imaging and motion parameters estimation algorithm with azimuth-dechirping and the second-order keystone transform applied," *IEEE J. Select. Topics Appl. Earth Observ. Remote Sensing*, Vol. 8, 3967–3976, 2015.
5. Li, G., X. G. Xia, and Y. N. Peng, "Doppler keystone transform for SAR imaging of moving targets," *IEEE Cong. Image Signal Process.*, Vol. 4, 716–719, 2008.
6. Yang, J., C. Liu, and Y. Wang, "Imaging and parameter estimation of fast-moving targets with single-antenna SAR," *IEEE Geosci. Remote Sensing Lett.*, Vol. 11, 529–533, 2014.
7. Yang, J., C. Liu, and Y. Wang, "Detection and imaging of ground moving targets with real SAR data," *IEEE Trans. Geosci. Remote Sensing*, Vol. 53, 920-932, 2015.
8. Xu, R., D. Zhang, D. Hu, X. Qiu, and C. Ding, "A novel motion parameter estimation algorithm of fast moving targets via single-antenna airborne SAR system," *IEEE Geosci. Remote Sensing Lett.*, Vol. 9, 920–924, 2012.
9. Zhang, X., G. Liao, S. Zhu, C. Zeng, and Y. Shu, "Geometry-information-aided efficient radial velocity estimation for moving target imaging and location based on Radon transform," *IEEE Trans. Geosci. Remote Sensing*, Vol. 53, 1105–1117, 2015.
10. Arii, M., "Efficient motion compensation of a moving object on SAR imagery based on velocity correlation function," *IEEE Trans. Geosci. Remote Sensing*, Vol. 52, 936–946, 2014.
11. Barbarossa, S. and V. Petrone, "Analysis of polynomial-phase signals by the integrated generalized ambiguity function," *IEEE Trans. Signal Process.*, Vol. 45, 316–327, 1997.
12. Barbarossa, S., A. Scaglione, and G. B. Giannakis, "Product high-order ambiguity function for multicomponent polynomial-phase signal modeling," *IEEE Trans. Signal Process.*, Vol. 46, 691–708, 1998.
13. Zhou, F., R. Wu, M. Xing, and Z. Bao "Approach for single channel SAR ground moving target imaging and motion parameter estimation," *IET Radar Sonar Navig.*, Vol. 1, 59–66, 2007.
14. Sun, H. B., G. S. Liu, H. Gu, and W. M. Su, "Application of the fractional Fourier transform to moving target detection in airborne SAR," *IEEE Trans. Aero. Electron. Syst.*, Vol. 38, 1416–1424, 2002.
15. Ruegg, M., E. Meier, and D. Nuesch, "Capabilities of dual-frequency millimeter wave SAR with monopulse processing for ground moving target indication," *IEEE Trans. Geosci. Remote Sensing*, Vol. 45, 539–553, 2007.
16. Zhu, S., G. Liao, Y. Qu, X. Liu, and Z. Zhou, "A new slant-range velocity ambiguity resolving approach of fast moving targets for SAR system," *IEEE Trans. Geosci. Remote Sensing*, Vol. 48, 432–451, 2010.
17. Feng, Y., "GNSS three carrier ambiguity resolution using ionosphere-reduced virtual signals," *J. Geodesy.*, Vol. 82, 847–862, 2008.
18. Baumgartner, S. V. and G. Krieger, "Acceleration-independent along-track velocity estimation of moving targets," *IET Radar Sonar Navig.*, Vol. 4, 474–487, 2010.